

01 May 2012

Silver Coated Bioactive Glass Particles for Wound Healing Applications

A. W. Wren


A. Coughlan

P. Hassanzadeh

Mark R. Towler

Missouri University of Science and Technology, mtowler@mst.edu

Follow this and additional works at: https://scholarsmine.mst.edu/che_bioeng_facwork

 Part of the [Biochemical and Biomolecular Engineering Commons](#), and the [Biomedical Devices and Instrumentation Commons](#)

Recommended Citation

A. W. Wren et al., "Silver Coated Bioactive Glass Particles for Wound Healing Applications," *Journal of Materials Science: Materials in Medicine*, vol. 23, no. 5, pp. 1331 - 1341, Springer, May 2012.

The definitive version is available at <https://doi.org/10.1007/s10856-012-4604-8>



This work is licensed under a [Creative Commons Attribution 4.0 License](#).

This Article - Journal is brought to you for free and open access by Scholars' Mine. It has been accepted for inclusion in Chemical and Biochemical Engineering Faculty Research & Creative Works by an authorized administrator of Scholars' Mine. This work is protected by U. S. Copyright Law. Unauthorized use including reproduction for redistribution requires the permission of the copyright holder. For more information, please contact scholarsmine@mst.edu.

Silver coated bioactive glass particles for wound healing applications

A. W. Wren · A. Coughlan · P. Hassanzadeh ·
M. R. Towler

Received: 29 September 2011 / Accepted: 27 February 2012 / Published online: 17 March 2012
© Springer Science+Business Media, LLC 2012

Abstract Bioactive glass particles (0.42SiO₂–0.15CaO–0.23Na₂O–0.20ZnO) of varying size (<90 μm and 425–850 μm) were synthesized and coated with silver (Ag) to produce Ag coated particles (P_{Ag}). These were compared against the uncoated analogous particles (P_{con.}). Surface area analysis determined that Ag coating of the glass particles resulted in increased the surface area from 2.90 to 9.12 m²/g (90 μm) and 1.09–7.71 m²/g (425–850 μm). Scanning electron microscopy determined that the Ag coating remained at the surface and there was little diffusion through the bulk. Antibacterial (*Escherichia coli*—13 mm and *Staphylococcus epidermidis*—12 mm) and antifungal testing (*Candida albicans*—7.7 mm) determined that small Ag-coated glass particles exhibited the largest inhibition zones compared to uncoated particles. pH analysis determined an overall higher pH consider in the smaller particles, where after 24 h the large uncoated and Ag coated particles were 8.27 and 8.74 respectively, while the smaller uncoated and Ag coated particles attained pH values of 9.63 and 9.35 respectively.

1 Introduction

The development of Bioglass by Hench in the 1960s has encouraged a succession of novel glass formulations and bioactive glass-based medical materials [1–4]. Originally developed as hard tissue replacement materials, the therapeutic effect of bioactive glasses stems from their ability to

release beneficial ions such as Ca²⁺, Na⁺, Zn²⁺, Sr²⁺, PO₃⁻⁴ in the body, which promote self-healing [1, 5–8]. Ion release from these materials results from the discontinuity of the Si–O–Si bonding in the glass due to the inclusion of network modifiers, which encourages the formation of non-bridging oxygen (NBO) groups. These NBO groups promote ion exchange processes thus facilitating bioactivity [5].

Bioactive glasses have been used in a wide range of orthopaedic applications including bone surrogates which can be distributed as particulates or particulate/paste composites. Bioactive glasses have also been used as coatings on metal prostheses [9] to encourage osteoinduction, as glass/ceramic scaffolds which facilitates cell growth and proliferation post implantation [10–13]. This study stems from previous work [14] and looks at coating bioactive glass particles with an antimicrobial surface composed of silver (Ag) as Ag₂O–SiO₂ glasses which can be difficult to produce by the traditional melt-quench method [15], however Ag-doped Bioglass based bone scaffolds have previously been produced by the ion exchange process [16]. Ag is known to have a wide antibacterial spectrum (against *E. coli* and *S. aureus* among other bacteria) and to be relatively safe to humans [17, 18]. Silver-based antimicrobial agents exhibit low toxicity of the active Ag ion to human cells, as well as it being a long-lasting biocide with high thermal stability and low volatility [17].

This work looks at determining the effect of coating the glass surface with Ag and also the antimicrobial properties of the glasses with respect to two species of prokaryotic organisms (*E. coli*, *S. epidermidis*), and one eukaryotic species, an opportunistic pathogenic fungi (*C. albicans*) which has been isolated from the skin and mucus membranes of healthy individuals. Both *E. coli* and *S. epidermidis*

A. W. Wren (✉) · A. Coughlan · P. Hassanzadeh ·
M. R. Towler
Inamori School of Engineering, Alfred University, Alfred,
NY 14802, USA
e-mail: wren@alfred.edu

have been implicated in septic complications relating to osteomyelitis and joint infection previously [19]. Osteomyelitis caused by *Candida* spp is relatively rare, however its prevalence is on the increase. Reports on 77 cases of *Candida* osteomyelitis found that the most affected bones were the vertebrae (31 cases, 40 %), and the sternum (6 cases, 8 %) with the remaining including the femur, mandible, clavicular joint, hand, hip and one case of *Candida* affected the foot bone [20]. Studies by Miller et al. found 59 cases of *Candidal* vertebral osteomyelitis in the literature. Osteomyelitis with *Candida* may occur in patients who have severely compromised host-defense mechanisms or who are receiving long standing intravenous therapy. Other factors that predispose patients to systemic infection is immunosuppression during cancer therapy, organ transplant, indwelling arterial/venous catheters and intravenous drug addiction with *C. albicans* being the most common cause [20]. Presently there is a need for new antifungal materials as the majority of fungi are resistant to antimicrobial drugs [21]. Current antifungal drug treatment includes two classes, polyenes (amphotericin B) and azoles (Fluconazole and Itraconazole) which are toxic to human tissues and have limited efficacy [21, 22].

The aim of this work sees to develop antimicrobial bioactive glasses of varying particle size, with a modified surface coating (Ag) and to determine the antimicrobial properties when compared to the uncoated glasses. Analysis was also carried out on the structural impact of having Ag as a coating on the glass surface.

2 Materials and methods

2.1 Glass synthesis

A glass with a composition $0.42\text{SiO}_2\text{--}0.15\text{CaO--}0.23\text{Na}_2\text{O--}0.20\text{ZnO}$ was used for this study. The glass was prepared by weighing out appropriate amounts of analytical grade reagents (Fisher Scientific, PA, USA) and ball milling (1 h). The mix was then oven dried (100°C , 1 h) and fired ($1,500^\circ\text{C}$, 1 h) in a platinum crucible and shock quenched in water. The resulting frit was dried, ground and sieved to retrieve two glass particle sizes, (a) $<90\ \mu\text{m}$ (small) and (b) $425\text{--}850\ \mu\text{m}$ (large).

2.2 Sample preparation

2.2.1 Preparation of Ag coatings

Ag coatings were produced by dissolving silver nitrate (AgNO_3) in 100 ml ethyl alcohol in solution (equivalent to 0.18 mol) for 1 h with the addition of moderate heating while spinning on a hot plate with a magnetic stirrer bar.

Two grams of each glass particle size was added to the dissolved AgNO_3 solution and left to spin for a further 3 h. After spinning, the glass particles were dried in an oven overnight and then heated to 300°C to remove residual NO_3^- Table 1.

2.3 Glass characterisation

2.3.1 X-ray diffraction (XRD)

Diffraction patterns were collected using a Siemens D5000 XRD Unit (Bruker AXS Inc., WI, USA). Glass powder samples were packed into standard stainless steel sample holders. A generator voltage of 40 kV and a tube current of 30 mA was employed. Diffractograms were collected in the range $10^\circ < 2\theta < 80^\circ$, at a scan step size 0.02° and a step time of 10 s. Any crystalline phases present were identified using JCPDS (Joint Committee for Powder Diffraction Studies) standard diffraction patterns.

2.3.2 Differential thermal analysis (DTA)

A combined differential thermal analyser-thermal gravimetric analyser (DTA-TGA) (SDT 2960 Simultaneous DSC-TGA, TA Instruments, DW, USA) was used to measure the glass transition temperature (T_g) for both glasses. A heating rate of $20^\circ\text{C min}^{-1}$ was employed using an air atmosphere with alumina in a matched platinum crucible as a reference. Sample measurements were carried out every 6 s between 30°C and $1,300^\circ\text{C}$.

2.3.3 Ag X-ray photoelectron spectroscopy (XPS)

XPS was performed using a PHI Quantera SXM Scanning X-ray Microprobe to analyze the surface chemistry, as well as the chemical state of the top few nanometers of the samples. Survey scans were used to monitor any the presence of any unexpected elements. The parameters for technique were $100\ \mu\text{m}$ spot size, 25 W, 15 kV, 240 eV pass energy, 0.5 eV step size, 3 sweeps, and a binding energy range of 0–1,100 eV. High resolution scans were then acquired of the binding energy regions associated with the Ag 3d peaks. Spot size, power, and voltage were held

Table 1 Description of glass/coated glasses used in this study

Glass description	Denotation
Uncoated– $90\ \mu\text{m}$ particle size	$P_{con,S}$
Uncoated– $425\text{--}850\ \mu\text{m}$ particle size	$P_{con,L}$
Ag coated– $90\ \mu\text{m}$ particle size	PAg_S
Ag coated– $425\text{--}850\ \mu\text{m}$ particle size	PAg_L

consistent, however, the pass energy and step size were reduced to 55 and 0.05 eV respectively, and the number of sweeps was raised to 5. All data was normalized based on the C1 s peak position of 284.8 eV.

2.3.4 Advanced surface area and porosity

In order to determine the surface area (SA) of each glass and any changes occurring after coating with Ag, advanced surface area and porosimetry, Micromeritics ASAP 2020 (Micromeritics Instrument Corporation, Norcross, USA) was employed. Approximately 60 mg of each glass sample was analyzed and the specific SA was calculated using the Brunauer–Emmett–Teller (BET) method.

2.3.5 SEM and energy dispersive X-ray analysis (EDX)

Backscattered electron (BSE) imaging was carried out with an FEI Co. Quanta 200F environmental scanning electron microscope. Additional compositional analysis was performed with an EDAX genesis energy-dispersive spectrometer. All EDS spectra were collected at 20 kV using a beam current of 26 nA. Quantitative EDS spectra were subsequently converted into relative concentration data.

2.4 Anti-microbial testing

2.4.1 Antibacterial testing

The antibacterial activity of the glass samples was evaluated against *E. coli* strain ATCC 8739, using the agar diffusion method. Luria agar and broth were used for the culture of *E. coli*, which was grown aerobically at 37° C. *S. epidermidis* strain ATCC 14990 was also used and was cultured in BHI agar and broth.

2.4.2 Antifungal testing

The antifungal activity of the glass samples was evaluated against *C. albicans* strain ATCC 18804, using the agar diffusion method. YM agar and broth were used for the culture of *C. albicans*.

2.4.3 Antimicrobial analysis

Preparation of the agar disc-diffusion plates involved seeding agar plates with a sterile swab dipped in a 1/50 dilution of the appropriate 16 h culture of bacteria. Samples of each glass ($n = 3$) of each particle size were placed on the inoculated plates and the plates were cultured for 24 h at 37° C (bacteria) and 30° C (fungi). The agar diffusion test was performed under standard laboratory sterile conditions in a fumigation hood using sterile swabs for

inoculation of bacteria/yeast. Calipers were used to measure zones of inhibition at three different diameters for each sample. Each sample was analyzed in triplicate and mean zone sizes \pm standard deviations were calculated.

$$\text{Inhibition Zone (mm)} = \frac{\text{Halo}\phi - \text{Disc}\phi}{2} \quad (1)$$

2.5 pH measurements

Changes in pH of solutions were monitored using a Corning 430 pH meter. Prior to testing, the pH meter was calibrated using pH buffer solution 4.00 ± 0.02 and 7.00 ± 0.02 (Fisher Scientific, Pittsburgh, PA). Sample solutions were prepared by exposing 5 m² surface area of each glass (Pcon._s, Pcon._L, PAg._s, PAg._L, where $n = 3$) in 10 ml de-ionised water. Measurements were recorded over $t = 0, 6, 24, 48, 72, 96, 120, 144$ and 168 h. De-ionised water was used as a control and was measured at each time period.

2.6 Statistical analysis

One-way analysis of variance (ANOVA) was employed to compare the antimicrobial efficacy of the experimental materials in relation to (1) uncoated and Ag-coated glasses (2) particle size of the uncoated and Ag-coated glasses. Comparison of relevant means was performed using the post hoc Bonferroni test. Differences between groups were deemed significant when $P \leq 0.05$.

3 Results and discussion

Initial work on these materials includes characterization with respect to the uncoated (Pcon.) and Ag-coated (PAg) glasses. XRD was initially performed on the glass at each processing stage. From Fig. 1a it is evident that no crystallinity is present in the starting material (Pcon.). Figure 1b shows the presence of crystalline species after spinning in AgNO₃ for 3 h which was subsequently identified as AgNO₃. Figure 1c shows the Ag-coated glass (PAg) after heating for 3 h and presents crystalline peaks which are predominantly associated with Ag. The glass also retains its characteristic amorphous hump post heat treatment in addition to the Ag crystalline species.

A thermal profile of each glass was determined using DTA in order to determine any structural changes as a result of the Ag surface modification. From Fig. 2a it is evident that the glass transition temperature (T_g) of the uncoated (Pcon.) glass is 540° C while the Ag coating reduced the T_g to 530° C. A similar trend was observed with the crystallization temperatures (T_c) where the Ag coating slightly reduced the T_{c1} and T_{c2} from 586 to 577° C

Fig. 1 XRD of (a) *Pcon* glass, (b) glass post-spinning in AgNO_3 and (c) after heat treatment (300°C)—*PAg*

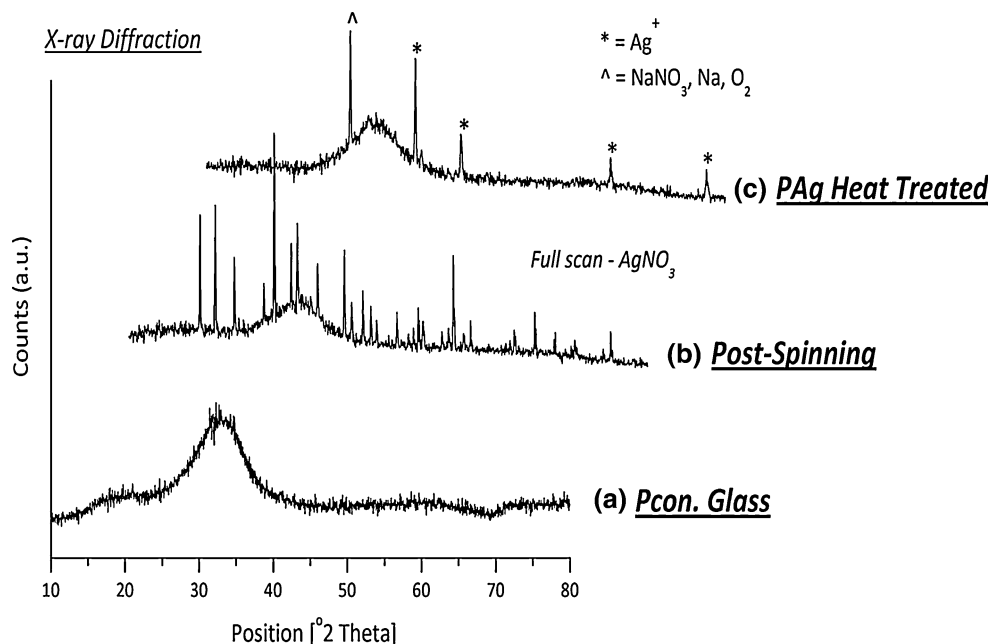
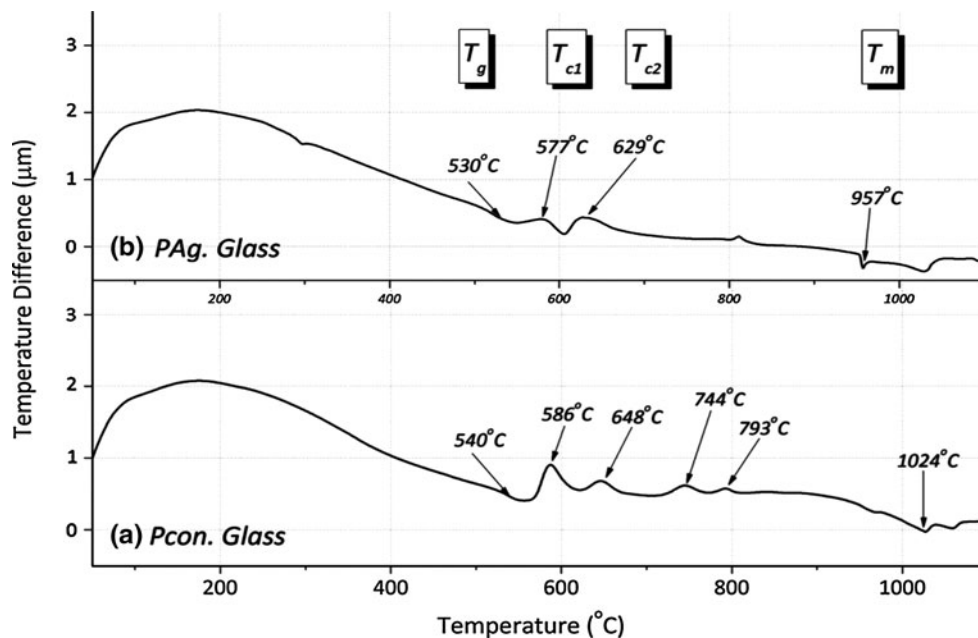


Fig. 2 DTA of glass **a** before coating (*Pcon.*) and **b** after Ag-coating (*PAg*)



and 648 to 629°C respectively. The melting temperature also decreased from 1024 to 957°C when coated with Ag (*PAg*). This may be a result of Ag slightly depolymerising the Si-OH^- groups on glass surface resulting in the glass requiring less thermal energy to decompose/crystallize in comparison to the uncoated glass (*Pcon.*).

XPS was employed to confirm the composition of each glass (*Pcon.*, *PAg*) and also to determine the chemical state of the Ag surface coating. Figure 3 presents the composition of the glasses. Figure 3a shows the composition of *Pcon.* which was found to contain Na , Zn , O , Ca and

Si , which are present in the starting composition. Some carbon (C) was also detected which arises from the substrate used for mounting samples in the instrument. Figure 3b presents the survey scan for *PAg*. From Fig. 3b it can be observed that Na , Zn , O , Ca , Si and Ag are present. It is evident also that the coating of Ag has reduced the peak intensity of each of the other elements present when compared to *Pcon.* High resolution XPS was also performed in order to determine the chemical state of Ag and also to determine any structural changes to the glass. Figure 4 shows the high resolution scans of O , Na and Ag .

Fig. 3 XPS survey of glass **a** before coating (*Pcon.*) and **b** after Ag-coating (*PAg*)

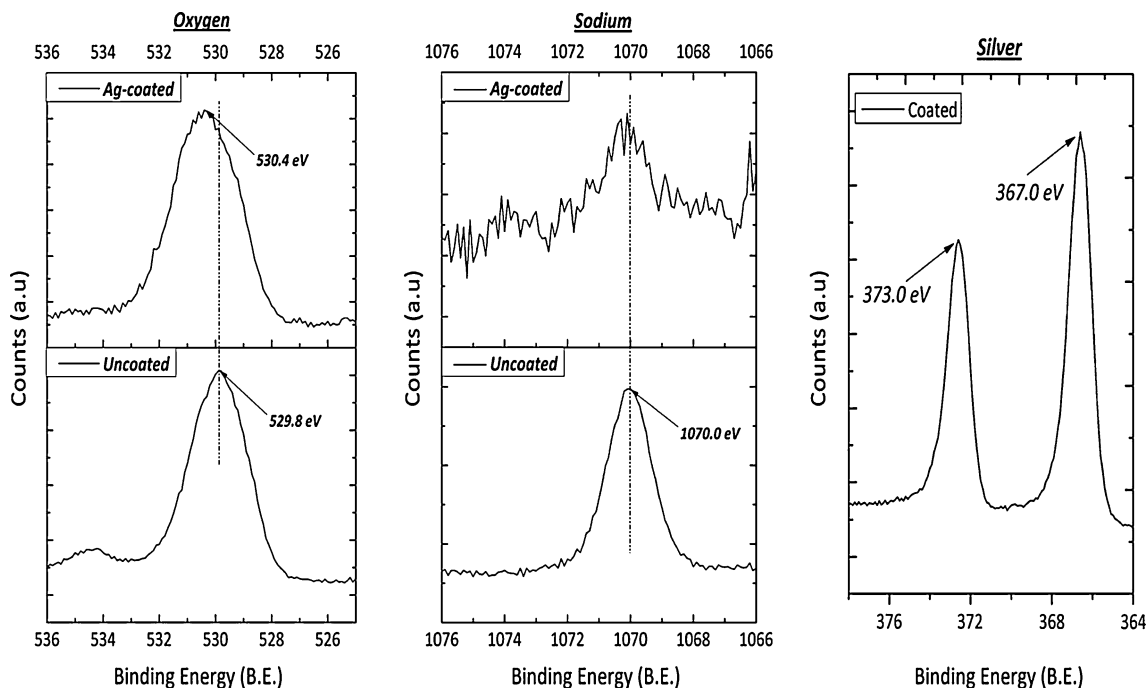
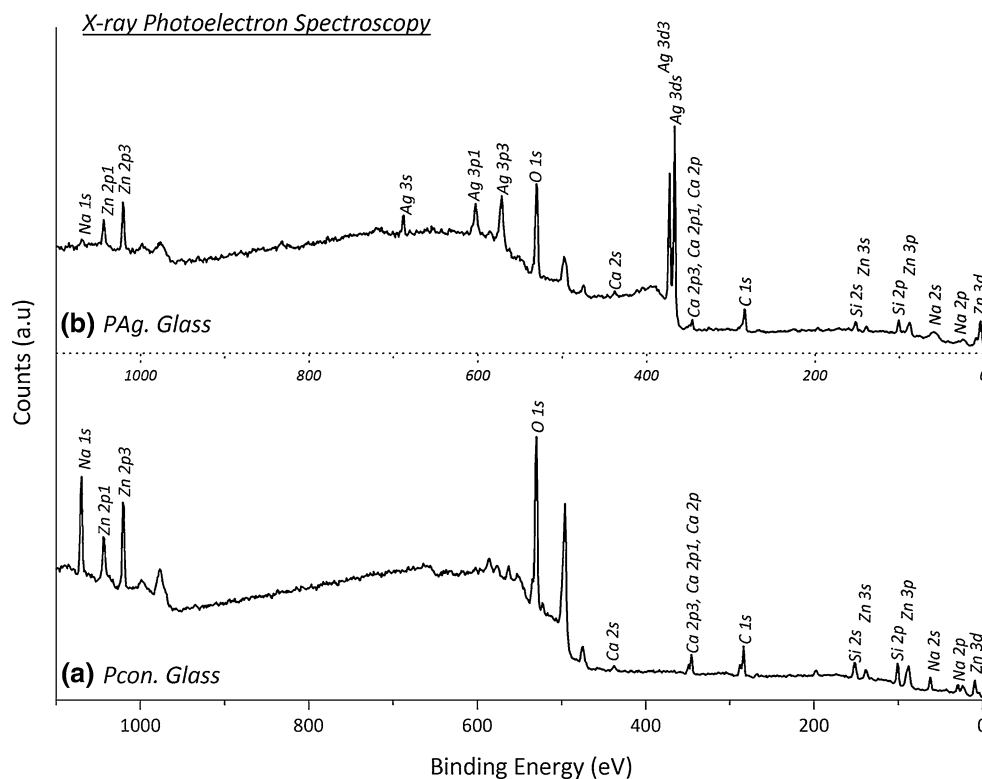


Fig. 4 High resolution XPS of oxygen, sodium and silver

The high resolution scan of O_{1s} shows that the binding energy (B.E.) shifted from 529.8 eV for the uncoated glass (*Pcon.*) to 530.4 eV for the Ag-coated glass (*PAg*). This shift is indicative of an increase in Si–O–Si groups while a

reduction in the BE is characteristic of an increase in NBO groups [4]. It is also evident that the Ag-coating (*PAg*) substitutes partly for the surface Na as the Na_{1s} signal is far less defined and resolved than the uncoated (*Pcon.*)

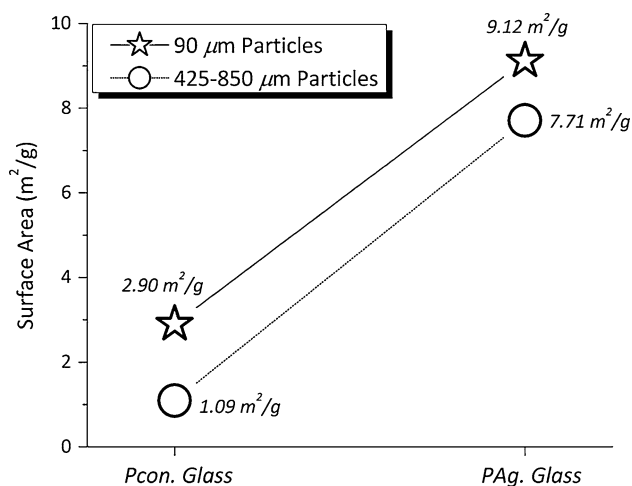


Fig. 5 BET surface area of 90 μm and 425–85 μm particles before and after Ag-coating

signal present at 1070.0 eV. The Ag $3d$ signal arises as a doublet with peaks being presented at 367.0–373.0 eV, which represent Ag $3d_{5/2}$ and Ag $3d_{3/2}$ which corresponds predominantly to AgO and Ag₂O [23, 24].

Surface area of the glass particles which were ground to two particle sizes (90 μm , 425–850 μm) was calculated using advanced surface area and porosity both before and after Ag-coating. Figure 5 shows the surface area results of Pcon. and PAg. It is evident that the Pcon. had a much lower surface area than the PAg glass. The 90 μm particles increased in surface area from 2.90 to 9.12 m²/g when

coated with Ag and the 425–850 μm particles increased from 1.09 to 7.71 m²/g. The increase in surface area may be attributed to the adsorption of Ag onto the surface of the PAg glass particles. Another contributing factor to the increased surface area of PAg may be the processing of the particles whereby during spinning in a liquid medium the glasses will likely grind under constant friction thereby reducing the particle size. Therefore the increased surface area may be as a result of the Ag coating in addition to the method of processing. However, by having a reduced particle size the increased exposed surface area of the glass will likely result in greater dissolution of the glass particles and thus facilitate greater release of therapeutic ions.

SEM and EDX was employed in order to investigate the surface and bulk composition of the glass particles. For this study the large Ag-coated (PAg_L) and uncoated (Pcon_L) particles were used. Glass particles were mounted in epoxy and polished prior to analysis by SEM. Figure 6 shows an image of PAg_L under the SEM. EDX was performed on the uncoated particle (Pcon_L) and is presented in Fig. 3a, while the Ag-coated glass (PAg_L) was analysed at the particle interior (Fig. 3b) and at the particle surface (Fig. 3c). EDX of Pcon_L shows the basic composition of the glass whereby Ca, Si, Na, Zn and O were present as expected. When analysing PAg_L with EDX it was found that the interior of the glass particle contained the same elements and quantitatively the composition was nearly identical to the Pcon_L glass. Analysis of the PAg_L surface found that the Ag was surface-bound and did not diffuse through the bulk of the material.

Fig. 6 EDX analysis of (a) uncoated Pcon. and (b, c) Ag coated PAg. glass

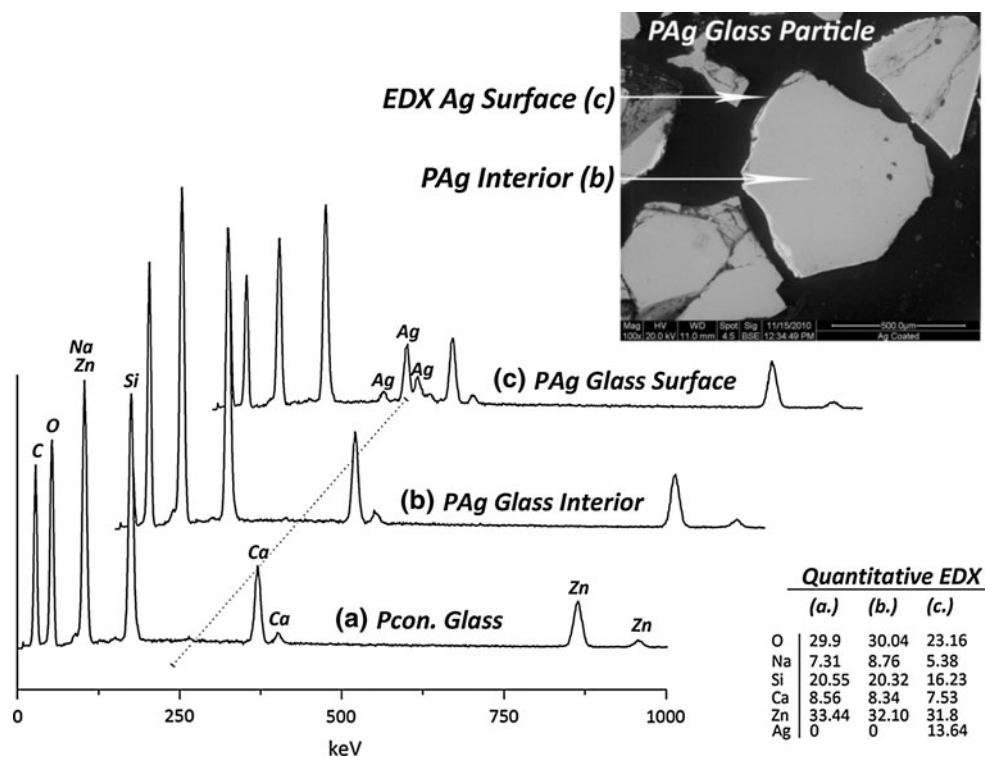
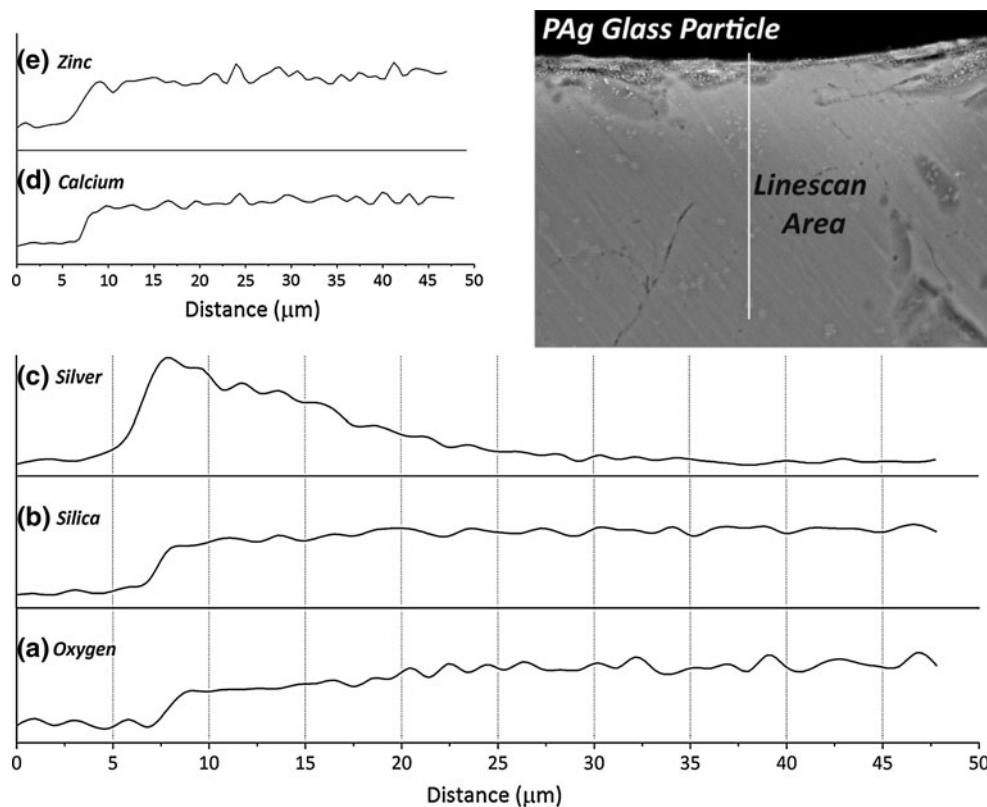


Fig. 7 Linescan EDX analysis of Ag coated PAg glass



EDX was used to further investigate the adsorption of Ag where an elemental line-scan was performed extending from the surface through to the centre of the particle. In particular the distribution of O and Si were compared with Ag. It was found that the concentration of both O and Si was reduced at the surface of the glass (Fig. 7a, b) which lies at $\sim 7.5 \mu\text{m}$, in comparison to the levels presented in the bulk of the glass, at around $40 \mu\text{m}$. A similar trend was found with Ca and Zn (Fig. 7d, e) where their concentration was higher in the bulk of the sample than at the surface. In Fig. 7c it is evident that the Ag concentration peaks at the glass surface, around $7.5 \mu\text{m}$, and decreases to a small fraction of this concentration at $\sim 40 \mu\text{m}$ into the bulk. Analysis of the glass particles determined that the Ag coating is predominantly surface-bound which is predominantly in the state of AgO, Ag₂O.

Antibacterial testing was performed using the agar-diffusion method using two strains of bacteria *E. coli* (gram -ve) and *S. epidermidis* (gram +ve). The spread plate method was used to determine the antibacterial activity of each glass at each particle size. Both bacteria used in this study are pathogens commonly found in a surgical environment; however, *S. epidermidis* has also been known to form biofilms on the surfaces of implantable medical devices [25, 26]. Glass particles were tested using the agar diffusion method where both large and small particles were tested in both bacterial strains. In relation to the large particles, the

uncoated control (*Pcon.L*) did not show any antibacterial properties when tested in either bacterium. The Ag-coated large particles (*PAg.L*) exhibited antibacterial properties in both bacteria. Inhibition zones observed were $4.19 \pm 0.66 \text{ mm}$ when tested in *E. coli*, and $1.95 \pm 0.27 \text{ mm}$ when tested in *S. epidermidis*. When considering the small control particles (*Pcon.S*), an antibacterial effect was evident when tested in *S. epidermidis*, where an inhibition zone of $3.95 \pm 0.91 \text{ mm}$ was observed. The most prominent antibacterial effect was observed with the small Ag-coated glass particles (*PAg.S*) where an inhibition zone of $13.12 \pm 0.73 \text{ mm}$ was observed using *E. coli* and an inhibition zone of $12.06 \pm 1.23 \text{ mm}$ was found using *S. epidermidis*. Statistical analysis was performed to compare the antibacterial effect of the uncoated glass (*Pcon.*) with the Ag-coated glasses (*PAg.*) and is presented in Table 2. At each stage the Ag-coated glasses exhibited a significant increase in

Table 2 Statistical analysis* comparing uncoated (*Pcon.*) with Ag-coated (*PAg.*) glasses

	<i>E. coli</i>		<i>S. epidermidis</i>	
	<i>PAg.L</i>	<i>PAg.S</i>	<i>PAg.L</i>	<i>PAg.S</i>
<i>Pcon.L</i>	0.000	0.000	0.000	0.000
<i>Pcon.S</i>	0.000	0.000	0.000	0.000

Significant at $P = 0.05$ level

antibacterial properties ($P = 0.000$) in both *E. coli* and *S. epidermidis*. The effect of particle size was also analysed by statistical analysis (Table 3) and it was found also that

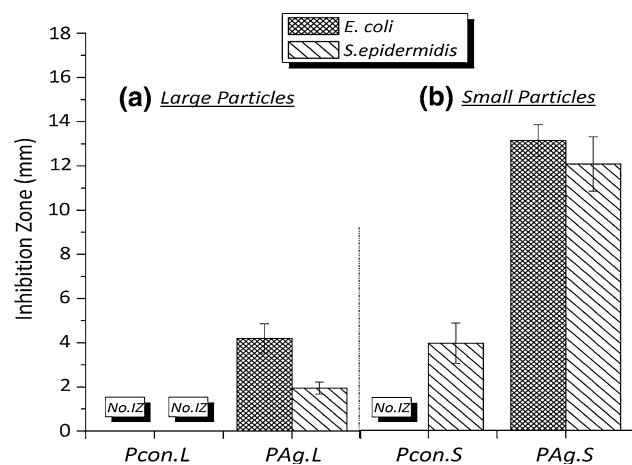


Fig. 8 Antibacterial testing of (a) large particles and (b) small particles in *E. coli* and *S. epidermidis*

at each stage the smaller particles (Pcon.S and PAg.S) had a significantly greater antibacterial response ($P = 0.000$) than the larger particles (Pcon.L and PAg.L) with the exception of (Pcon.S and Pcon.L) when tested in *E. coli*. There was no significant change in this instance as no inhibition zones were observed for either glass Figs. 8 and 9.

The mechanism of action of Ag includes uncoupling of respiratory electron transport processes, collapse of the proton-motive forces across the cytoplasm membrane and interferes with membrane permeability; membrane bound enzymes and proteins [27, 28]. Studies by Wang and

Table 3 Statistical analysis* comparing particle size effects in each bacteria

	<i>E. coli</i>		<i>S. epidermidis</i>	
	Pcon.S	PAg.S	Pcon.S	PAg.S
Pcon.L	1.000	0.000	0.000	0.000
PAg.L	0.000	0.000	0.000	0.000

Significant at $P = 0.05$ level

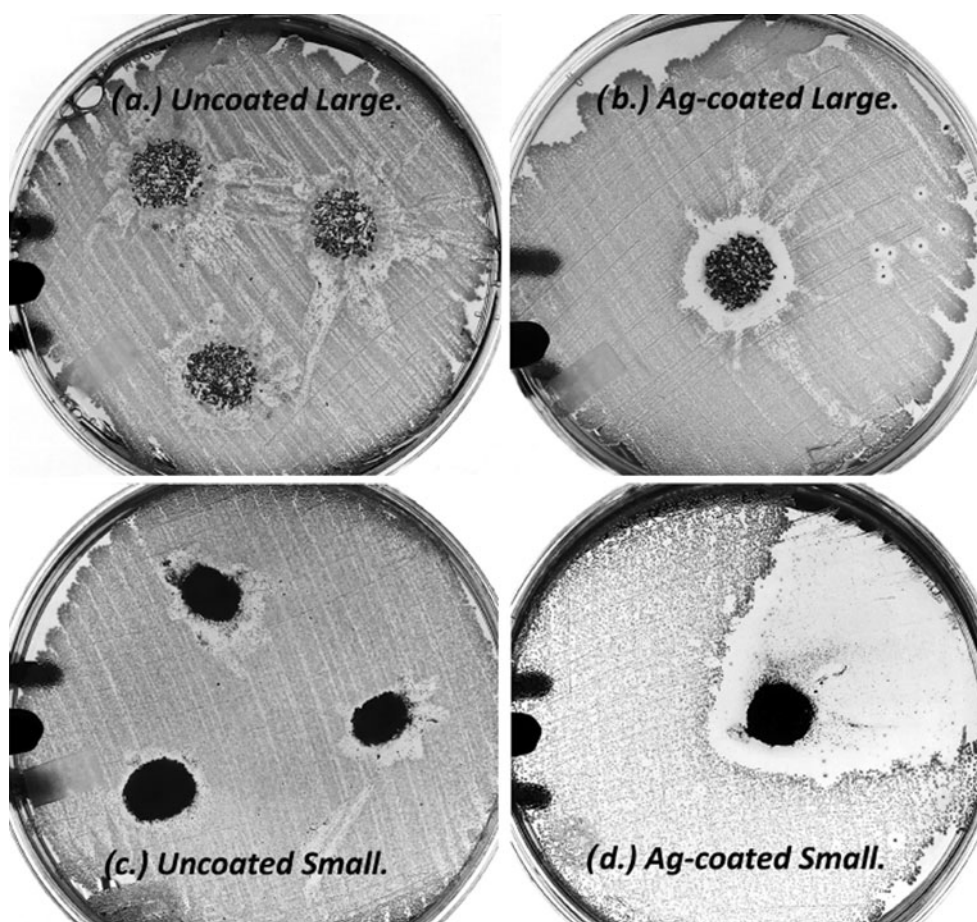


Fig. 9 Antibacterial testing of (a) Pcon.L, (b) PAg.L, (c) Pcon.S and (d) PAg.S in *E. coli*

Fig. 10 Antibacterial testing of Pcon. and PAg. in *C. albicans*

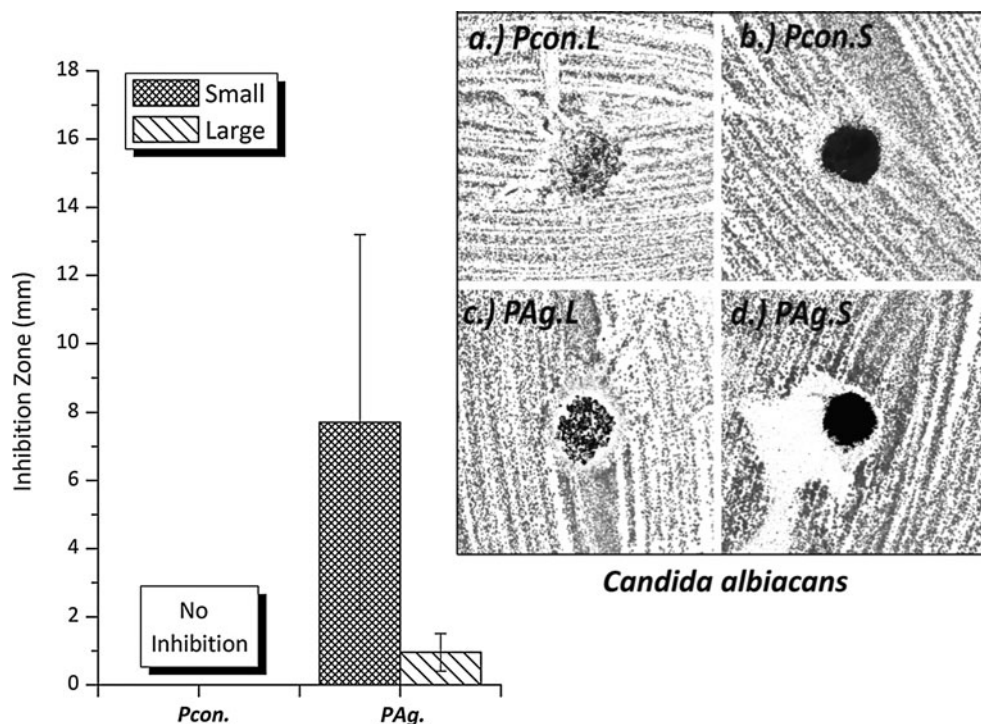
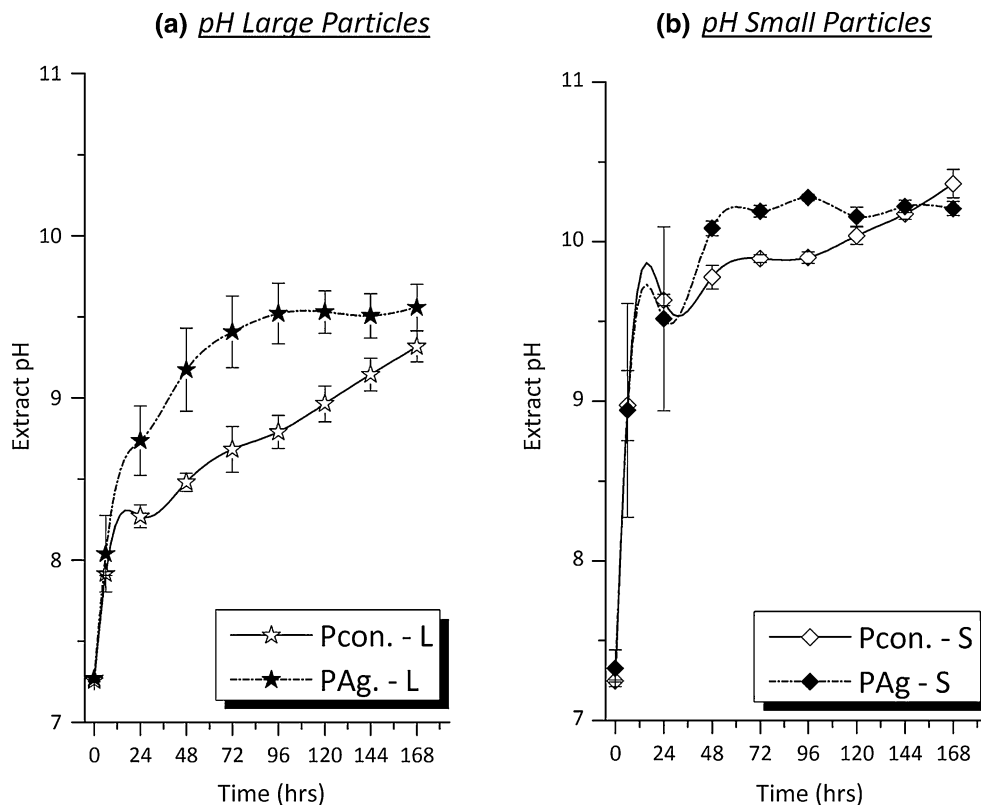


Fig. 11 pH measurements considering (a) large particles and (b) small particles



coworkers [28] on the effect of Ag ion on the cell walls of *E. coli* and *S. epidermidis* determined that the difference in cell wall structure resulted in differences in bacterial

response to Ag, where the thick peptidoglycan walls of *S. epidermidis* proved more difficult to breakdown, as was observed in this study.

In addition to bacteria, a pathogenic strain of fungi was investigated as the eukaryotic cell structure of fungi differs to that of the prokaryotic bacterial cell. The organism used for testing was *C. albicans* and followed a similar trend to the bacterial testing, where the control glass ($P_{con,L}$ and $P_{con,S}$) particles did not exhibit any antifungal properties while the Ag coated materials did. PAg_S exhibited the largest inhibition zones 7.7 ± 5.5 mm while the larger Ag particles, PAg_L , showed inhibition zones of 0.96 ± 0.55 mm. In this instance, similarly to the bacterial testing, the smaller particles resulted in significantly ($P = 0.001$) larger inhibition zones than the large glass particles. This increase in antimicrobial properties is due to the greater surface area of the smaller glass particles as evinced by surface area analysis. It is also likely that Ag surface deposition and release is proportional to the exposed surface area, which results in a higher of Ag release and subsequent ion release rate Fig. 10.

A determining factor in the antimicrobial response is the effect of the surrounding pH. For this study the surrounding pH was measured from $t = 0$ up to $t = 168$ h (7 days). Considering the large glass particles ($P_{con,L}$ and PAg_L), the initial pH of the aqueous medium was determined to be 7.26 and 7.27 for each sample respectively. After 24 h of incubation the pH increased to 8.27 ($P_{con,L}$) and to 8.74 (PAg_L). At each stage the solution containing the Ag coated particles achieved a higher pH than the uncoated glass particles, however at $t = 168$ there was little difference in pH between $P_{con,L}$ (9.32) and PAg_L (9.56). Regarding the smaller particles, the pH at $t = 0$ was similar to that of the large particles, however at $t = 24$ h the pH was greater for both $P_{con,S}$ and PAg_S at 9.63 and 9.52 respectively. Similarly to the large particles the difference at $t = 168$ h was insignificant at 10.36 and 10.21 for $P_{con,S}$ and PAg_S respectively.

Further testing will be necessary to completely determine the effect of pH on bacterial growth, in particular, *S. epidermidis*, which may be more susceptible to changes in local pH. This is evinced by the lack of any antibacterial effects in $P_{con,L}$, as opposed to their being an antibacterial effect with $P_{con,S}$ which presented a higher pH value. However this may also be a particle size effect. Future work will also include analysis in simulated body fluid to determine whether the Ag coating inhibits the ability of this bioactive glass to induce mineral formation, and whether this mineral is altered compared to that formed on the control uncoated glass. Additionally inductively coupled plasma optical emission spectroscopy will be performed to determine the rate of ion release for each component of these materials, in addition to cytotoxicity analysis will be conducted as previous studies have demonstrated that low Ag concentration can encourage cell proliferation of human cell lines [16] Fig. 11.

References

- Hench LL. The story of bioglass. *J Mater Sci Mater Med*. 2006;17:967–78.
- Hench LL, Peitl O, Zanotto ED. Highly bioactive P_2O_5 - Na_2O - CaO - SiO_2 glass ceramics. *J Non Cryst Solids*. 2001;292:115–26.
- Verne E, Di Nunzio S, Bosetti M, Appendino P, Vitale Brovarone C, Maina G, Cannas M. Surface characterization of silver-doped bioactive glass. *Biomaterials*. 2005;26:5111–9.
- Wren AW, Laffir FR, Kidari A, Towler MR. The structural role of titanium in Ca - Sr - Zn - Si / Ti glasses for medical applications. *J Non Cryst Solids*. 2010;357(3):1021–6.
- Serra J, Gonzalez P, Liste S, Chiussi S, Leon B, Perez-amor M, Ylanen HO, Hupa M. Influence of the non-bridging oxygen groups on the bioactivity of silicate glasses. *J Mater Sci Mater Med*. 2002;13:1221–5.
- Kokubo T, Takadama H. How useful is SBF in predicting in vivo bone bioactivity. *Biomaterials*. 2006;27:2907–15.
- Rico H, Villa LF. Zinc, a new coherent therapy for osteoporosis. *Calcif Tissue Int*. 2000;67:422–3.
- Balamurugan A, Balossier G, Kannan S, Michel J, Rebelo AHS, Ferreira JMF. Development and in vitro characterization of sol-gel derived CaO - P_2O_5 - SiO_2 - ZnO bioglass. *Acta Biomater*. 2007;3:255–62.
- Piscanec S, Ciacchi LC, Vesselli E, Comelli G, Sbaizero O, Meriani S, De Vita A. Bioactivity of TiN-coated titanium implants. *Acta Mater*. 2004;52:1237–45.
- Ochoa I, Sanz-Herrera JA, García-Aznar JM, Doblaré M, Yunos DM, Boccaccini AR. Permeability evaluation of 45S5 bioglass®-based scaffolds for bone tissue engineering. *J Biomech*. 2009;42(3):257–60.
- Chen QZ, Thompson ID, Boccaccini AR. 45S5 Bioglass®-derived glass-ceramic scaffolds for bone tissue engineering. *Biomaterials*. 2006;27(11):2414–25.
- Peter M, Binulal NS, Nair SV, Selvamurugan N, Tamura H, Jayakumar R. Novel biodegradable chitosan-gelatin/nano-bioactive glass ceramic composite scaffolds for alveolar bone tissue engineering. *Chem Eng J*. 2010;158(2):353–61.
- Jones JR, Ehrenfried LM, Hench LL. Optimising bioactive glass scaffolds for bone tissue engineering. *Biomaterials*. 2006;27(7):964–73.
- Wren AW, Akgun B, Adams B, Coughlan A, Mellott NP, Towler MR. Characterization and antibacterial efficacy of silver-coated Ca - Na - Zn - Si / Ti glasses. *J Biomater Appl*. 2011;7(3):1–4.
- Kawashita M, Tsuneyama S, Miyaji F, Kokubo T, Kozuka H, Yamamoto K. Antibacterial silver-containing silica glass prepared by solgel method. *Biomaterials*. 2000;21:393–8.
- Newby PJ, El-Gendy R, Kirkham J, Yang XB, Thompson ID, Boccaccini AR. Ag-doped 45S5 Bioglass (R)-based bone scaffolds by molten salt ion exchange: processing and characterisation. *J Mater Sci Mater Med*. 2011;22(3):557–69.
- Lee S-B, Otgonbayar U, Lee J-H, Kim K-M, Kim K-N. Silver ion-exchanged sodium titanate and resulting effect on antibacterial efficacy. *Surf Coat Technol*. 2010;205(1):S172–6.
- Husheng J, Wensheng H, Liqiao W, Bingshe X, Xuguang L. The structures and antibacterial properties of nano- SiO_2 supported silver/zinc-silver materials. *Dent Mater*. 2008;24:244–9.
- Axford JS. Joint and bone infections. *Medicine*. 2006;34(10):405.
- Arias F, Mata-Essayag S, Landaeta ME, de Hartung Capriles C, Perez C, Nunez MJ, Carvajal A, Silva M. *Candida albicans* osteomyelitis: case report and literature review. *Int J Infect Dis*. 2004;8:307–14.
- Pastor L, García-Domenech R, Gálvez J, Wolski S, García MD. New antifungals selected by molecular topology. *Bioorg Med Chem Lett*. 1998;8(18):2577–82.

22. Jiang B, Bussey H, Roemer T. Novel strategies in antifungal lead discovery. *Cur Opin Microbiol.* 2002;5(5):466–71.
23. Lou N, Lixin M, Lizhong J, Zhan J, Wu Z, Wu D. Directly ultraviolet photochemical deposition of silver nanoparticles on silica spheres: preparation and characterization. *Mater Lett.* 2009; 63:154–6.
24. Akgun BA, Durucan C, Mellott NP. Effect of silver incorporation on crystallization and microstructural properties of sol–gel derived titania thin films on glass. *J Sol Gel Sci Technol.* 2011;58:277–89.
25. Qin Z, Zhang J, Hub Y, Chi Q, Mortensen NP, Quc D, Molin S, Ulstrup J. Organic compounds inhibiting *S. epidermidis* adhesion and biofilm formation. *Ultramicroscopy.* 2009;109:881–8.
26. Pallavicini P, Taglietti A, Dacarro G, Diaz-Fernandez YA, Galli M, Grisoli P, Patrini M, De Magistris GS, Zanoni R. Self-assembled monolayers of silver nanoparticles firmly grafted on glass surfaces: low Ag + release for an efficient antibacterial activity. *J Colloid Interface Sci.* 2010;350:110–6.
27. Balamurugan A, Balossier G, Laurent-Maquin D, Pina S, Rebelo AHS, Faure J, Ferreira JMF. An in vitro biological and antibacterial study on a sol–gel derived silver-incorporated bioglass system. *Dent Mater.* 2008;24:1343–51.
28. Yang X, Yang W, Wang Q, Li H, Wang k, Yang L, Liu W. Atomic force microscopy investigation of the characteristic effects of silver ions on *Escherichia coli* and *Staphylococcus epidermidis*. *Talanta.* 2010;81:1508–12.